IEEE Robotics and Automation Letters (RAL) paper presented at the
2020 IEEE/RSJ International Conference on Intelligent Robots and Systems (IROS)
October 25-29, 2020, Las Vegas, NV, USA (Virtual)

6-Axis Force/Torque Sensor with a Novel Autonomous Weight Compensating Capability for Robotic Applications

Yong Bum Kim[1], Dong-Yeop Seok[2], Seung Yeon Lee[2], Jaeyun Kim[2], Gitae Kang[2], Uikyum Kim[3] and Hyouk Ryeol Choi[2], Fellow, IEEE

Abstract— Force/Torque(F/T) sensing technology enables a dexterous robot control such as direct teaching, master-slave system, and pick-and-place task. In general, 6-axis F/T sensor is attached to the end-effector of the robot manipulator to assist in utilizing advanced robot systems. However, in actual applications, various tools such as robotic grippers, robotic hand, grinders are attached to the sensor and it causes F/T offsets with respect to the gravity. In this letter, Autonomous Weight Compensating(AWC) technique for 6-axis F/T sensor is presented. The proposed AWC technique can reduce the F/T offsets by estimating the F/T offsets through installed Inertial Measurement Unit(IMU) sensor. In this study, the 6-axis F/T are measured based on capacitance sensing scheme and to estimate the orientation of the sensor, a 9-axis IMU sensor is installed inside of the sensor. Then, the F/T offsets are calibrated via Artificial Neural Network(ANN) model. Finally, the performance of the proposed method is demonstrated through comparing the F/T data with both trained data and untrained data.

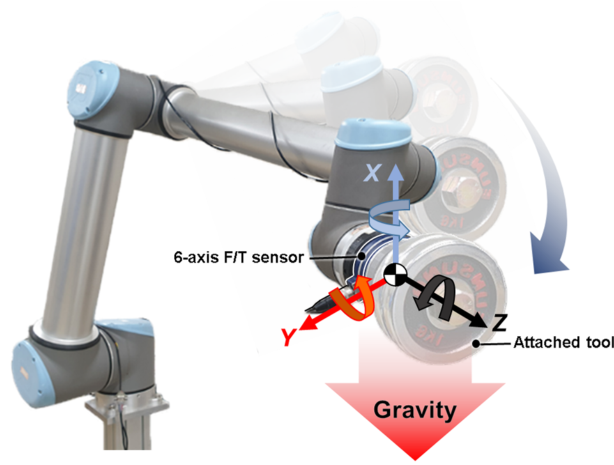

Fig. 1. 6-axis F/T offsets respected with the gravity.

I. INTRODUCTION

Nowadays, collaborative robots are designed to interact with humans to enhance performance and efficiency. Consequently, in order to achieve a safety in human-robot interaction, interaction sensing systems are prerequisite in the field of the advanced robot system. In particular, 6-axis Force/Torque (F/T) sensor is highlighted due to its valuable uses in the dexterous robot such as direct teaching, master-slave system, and safety system of the robot [1]-[4]. In this system, a 6-axis F/T sensor provides interaction forces from the objects. Moreover, a number of advanced robotic platforms such as robot manipulator, legged robot, and surgical robot have gradually embeded F/T sensor to their system [4]-[10].

Particularly, in the field of the robot manipulator, a 6-axis F/T sensor is a prerequisite to conduct dexterous tasks that aid the human-robot collaboration. However, apart from the price, size and sensing range, there is a significant function that the sensor need to complement. That is “Autonomous Weight Compensating (AWC)” function for the 6-axis F/T sensor. This function helps to measure pure interaction F/T. In other words, the 6-axis F/T sensors are generally influenced by gravity on the attached tools (Fig.1) and it disrupts to measure pure interaction F/T. Thus, to use the 6-axis F/T sensor on the purpose of interaction sensing, this F/T offsets need to be compensated.

Currently, to compensate F/T offsets from the attached tool, manual processes are conducted. A company called “Robotiq” provides a solution to compensate the 6-axis F/T offsets by conducting some manual works [11]. In their solution, to compensate the 6-axis F/T offsets, weight and center of mass are required and they are estimated through some manual steps. This group proposed three poses that are matched on each X, Y, and Z-axis with gravity. In the first pose, the X-axis of the tool is placed perpendicular to gravity. Thus, the X-axis force and Y-axis torque are acted in the first pose. Similarly, in the second pose, the Y-axis of the tool is located perpendicular to the gravity. In this pose, the Y-axis force and X-axis torque are given. In the third pose, the Z-axis of the tool is positioned parallel to gravity. Hence, only the Z-axis force is measured and is used to calculate the weight of the tool. Combining these F/T information, the weight and center of the mass are finally estimated.

This method is the most common process of compen-

This work was supported by the Technology Innovation Program (20001228, Development of Coaxial Drive Module for Collaborative Robot with Sensor SoC Technology) funded By the Ministry of Trade, Industry & Energy(MOTIE, Korea)

[1]Y. B. Kim with the School of Mechanical Engineering, Sungkyunkwan University, Suwon 440-746, South Korea. He is now with AIDIN ROBOTICS, Suwon, Korea, 440-746 (e-mail :ybkim@aidinrobotics.com).

[2]D.-Y. Seok, S. Y. Lee, J. Kim, G. Kang and H. R. Choi are with the School of Mechanical Engineering, Sungkyunkwan University, Suwon, Korea, 440-746 (e-mail :hrchoi@me.skku.ac.kr).

[3]U. Kim was with the School of Mechanical Engineering, Sungkyunkwan University, Suwon 440-746, South Korea. He is now with Korea Institute of Machinery and Materials, Deajeon 305-343, South Korea. (e-mail :ukkim@kimm.re.kr).

sating the 6-axis F/T offsets. However, this method could be very critical issue due to the requirement of human resource in the factory. Also, there are the possible errors introduced by human interventions. Dimes et al. proposed an optimal variable admittance control which includes the weight compensation algorithm [12]. The weight and center of mass are estimated by using attached 6-axis F/T sensor. According to their proposed method, manual processes are not required, but this technique demands additional computing time to obtain 6-axis F/T offsets.

Also, for some medical robotic systems 6-axis F/T sensors are used for haptic feedback, pressure control and user interaction. In this application, for accurate force and torque detection during operation, the tool's weight related force and torque must be subtracted [13], [14]. Kim et al. used 6-axis F/T sensor to develop bone fracture reduction robotic system to relieve the surgeon's physical load. However, the knob's gravity caused by the offset force deteriorate the robot's maneuverability in the interactive control. Thus, they introduced a gravity force compensation method which uses the 6-axis F/T sensor with the rotation matrix from the manipulator. However, this approach still needs to know the rotation matrix from the manipulator, thus the gravity compensation method cannot be independent to the robot system.

In this research, a novel AWC technique for the 6-axis F/T sensor is proposed which can solve the requirement of manual works and also, it also has benefit to reduce extra computing time for compensating 6-axis F/T offsets. Also, the proposed technique can simply realize by embedding a 9-axis IMU sensor into the 6-axis F/T sensor. In this letter, in regards to the 6-axis F/T sensing, previously developed capacitance sensing technology is used [6], [15] and an IMU sensor is installed to estimate the orientation of the sensor. Also, ANN model is introduced in estimating process of the F/T offsets.

The rest of the letter is organized as follows: The concept and configuration of the 6-axis sensor is presented in Section II. Section III introduces the calibration process using ANN model. Section IV addresses the evaluation processes of the proposed sensor. Finally, conclusions are presented in Section V.

II. CONCEPT OF 6-AXIS F/T SENSOR FOR AWC TECHNIQUE

A. Mechanical Structure of 6-axis F/T sensor

The proposed 6-axis F/T sensor consists of four mechanical parts and one signal processing board. Each part is assembled through a bolting connection without any bonding process. Figure 2 presents the configuration of the signal processing board and sensing plate. The air gap between the signal processing board and the sensing plate is created when the deformable plate is assembled to the bottom plate. In addition, the sensing electrode covers the entire edge of the PCB. Thus, the air gaps are generated parallelly and orthogonally. The capacitance sensing scheme is based on the orthogonal configuration of two conductive electrodes [16]. In this research, the sensing plate is connected to the ground which generates capacitance between the electrode of the signal processing board. Also, according to (1), (2), the flange effect is generated on parallel and orthogonal electrode.

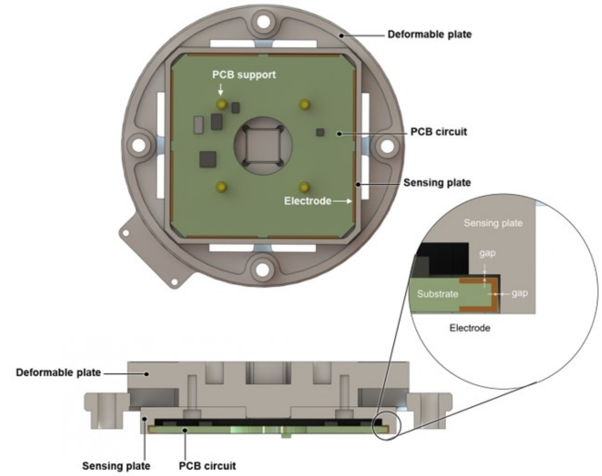

Fig. 2. Detailed configuration of generated sensing gap in vertical and horizontal direction.

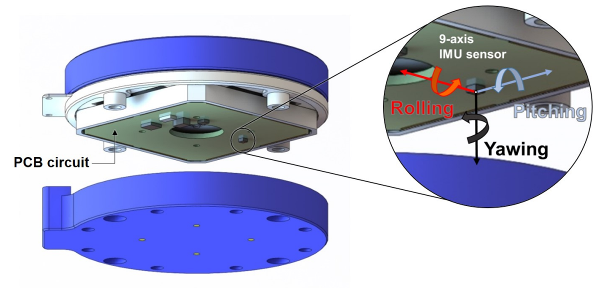

Fig. 3. Configuration of 9-axis IMU sensor installation.

$$\Delta C = \Delta C_{wr} + \Delta C_{fr} \tag{1}$$

$$\Delta C_{wr} = \varepsilon_0 \varepsilon_r \frac{\Delta A}{\Delta d}, \tag{2}$$

where ΔC denotes the change in capacitance, and ΔC_{wr} and ΔC_{fr} denote the capacitance variation in the covered area and the variation owing to the fringe effect, respectively. Additionally, ε_0 and ε_r represent the dielectric constant and the static relative permittivity. Furthermore, ΔA and Δd represent the change in the overlapping area and the distance between the two electrodes, respectively. Capacitance variation owing to the fringe effect can be derived as follows [6]

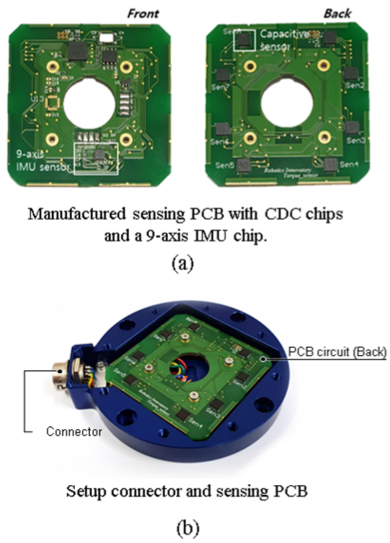

Fig. 4. Installation of sensing PCB. (a) CDC sensors and IMU sensor installed PCB design. (b) Connection of sensing PCB with the bottom plate.

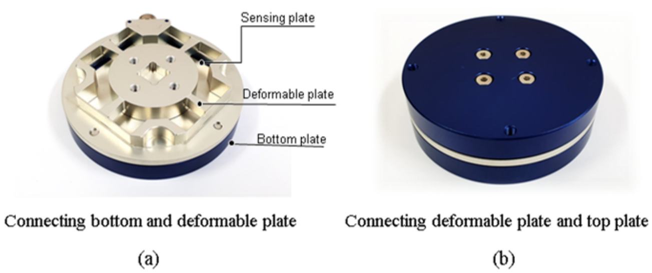

Fig. 5. Assembly of the 6-axis F/T sensor. (a) Assembly of deformable plate. (b) Fully assembled sensor.

$$\Delta C_{fr} = 2\varepsilon_0\varepsilon_r \left[\left(\frac{K'(k_{in}(d_0))}{K(k_{in}(d_0))} + \frac{K'(k_{out}(d_0))}{K(k_{out}(d_0))} \right) - \left(\frac{K'(k_{in}(d'))}{K(k_{in}(d'))} + \frac{K'(k_{out}(d'))}{K(k_{out}(d'))} \right) \right] \quad (3)$$

where $K(k)$ represents the complete elliptic integral. k_{in} and k_{out} represent the modulus, d_0 represents the initial distance, and $d' = d_0 - \Delta d$ [6].

In the manufactured signal processing board, it embeds eight CDC (Capacitance to Digital Converter) sensors on the backside and a 9-axis IMU sensor on the front side (Fig. 3). As a result, eight capacitance data, a 3-axis gyroscope, a 3-axis accelerometer, and a 3-axis magnetometer data can be obtained from the sensor PCB.

In order to optimize the capacitance variation with desired F/T, the deformable plate is analyzed as four cross-elastic beams with compliant beams. This analysis technique is introduced in the previous research [15].

B. Electrical component of 6-axis F/T sensor

1) Capacitance to 6-axis F/T: In this research, independent eight positive electrodes are located on the four

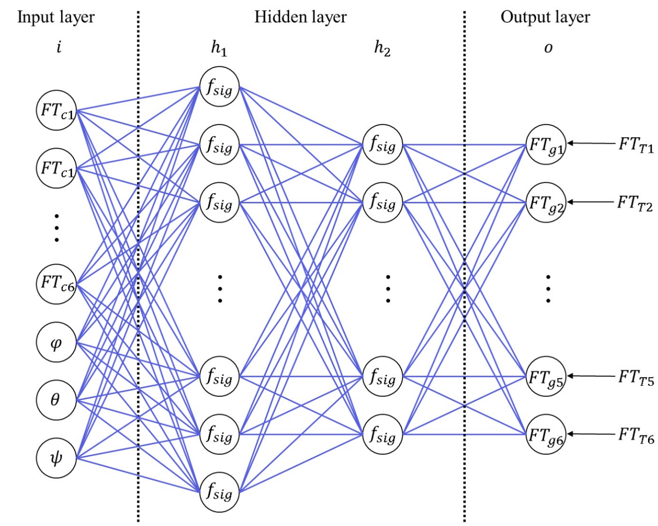

Fig. 6. Neural network of ANN model for compensating the F/T offsets from the attached tool.

edges of the signal processing board [8]. Therefore, it makes a total of eight independent capacitance variations associated with the deformation of 6-axis F/T. In order to minimize the outer electromagnetic interference on the sensor, the CDC sensors are placed near the sensing electrode.

But, capacitance varies non-linearly in regards to the distance variation. Thus, the non-linearity of each capacitance variation results to the phenomenon and inaccurate sensing of the result. To obtain the linearly converted data, commonly, the mathematical models are founded as an exponential or polynomial function. However, to derive entire relations of parallel and orthogonal deformation, a lot of computing time to solve high-level non-linearity fitting functions within the operating period is required. Furthermore, it needs to multiply the calibration matrix after the linear converting process. In this letter, we used a deep-learning method which was introduced in the previous paper in order to convert capacitance to 6-axis F/T along with the linear converting process of capacitance [17]. This method offers high performance for regression of data and a non-linear activation function is utilized for linear fitting. Thus, the eight capacitance data can successfully converted to the 6-axis F/T.

In regards to capacitance sensing, capacitance-to-digital (CDC) chip (AD7147, Analog Devices) are selected. The CDC chip provides a maximum sampling rate of 1.3 kHz and 16-bit resolution. The developed sensor installs eight CDC chips to satisfy the 1 kHz sampling rate, simultaneously. The digitalized capacitance data in the CDC chip is transferred to the MCU chip (STM32F103 series, ST) via a serial peripheral interface bus (SPI) communication interface.

2) IMU data to roll, pitch and yaw: The 9-axis IMU values are used to convert into the Euler angle of the

TABLE I

Specifications of the 6-axis F/T sensor

Quantity	Value	Unit
Diameter	82	mm
Height	25.5	mm
Weight	250	g
Force range	±500	N
Torque range	±20	Nm
Sampling rate	1000	Hz
Gyroscope Full-scale range	±500	°/s
Accelerometer Full-scale range	±4	g
Magnetometer Full-scale range	±4800	μT

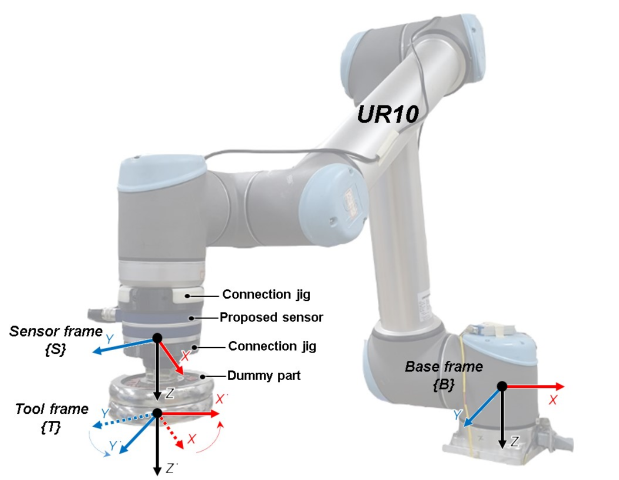

Fig. 7. Evaluation set-up used to obtain training data and untrained test data with UR10 manipulator.

end effector (φ, ϕ, and ψ) by using the equations below.

From the 3-axis gyroscope measurements, the orientation of the sensor can be estimate as follows

$$\varphi_g = \varphi_g + \int \Delta G_x dt \tag{4}$$

$$\phi_g = \phi_g + \int \Delta G_y dt \tag{5}$$

where, φ_g, ϕ_g are estimated φ, ϕ using gyroscope measurement. G_x and G_y represents X, Y-axial gyroscope measurements from the sensor.

From the 3-axis acceleration measurements, the orientation of can be estimate as follows

$$\varphi_a = atan\frac{A_y}{\sqrt{A_x^2 + A_z^2}} \tag{6}$$

$$\phi_a = atan\frac{-A_x}{\sqrt{A_y^2 + A_z^2}} \tag{7}$$

Here, φ_a, ϕ_a are estimated φ, ϕ using acceleration measurement. A_x and A_y represents X, Y-axial acceleration measurements from the sensor.

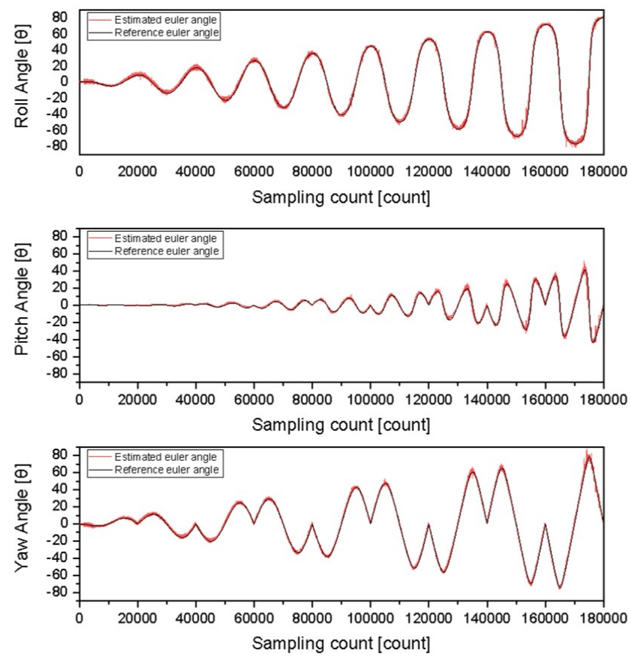

Fig. 8. Estimated euler angle: black line shows the reference Euler angle, red line shows the estimated Euler angle.

In this research, the complementary filter is used to estimate φ, ϕ.

$$\varphi = \alpha \cdot \varphi_a + \beta \cdot \varphi_g \tag{8}$$

$$\phi = \alpha \cdot \phi_a + \beta \cdot \phi_g \tag{9}$$

Here, α, β denote the gain for calculated φ, ϕ from gyroscope, acceleration measurement. And $\beta = 1 - \alpha$. Generally, α can calculate as follow:

$$\alpha = \frac{\tau}{\tau + \delta t}, \tag{10}$$

where τ is the desired time constant and δt means sampling frequency. In this letter, we set α as 0.96. Finally, Yaw angle is estimated using estimated φ, ϕ and magnetometer data as follows

$$Y_h = (M_y \cdot cos(\phi)) - (M_z \cdot sin(\phi)) \tag{11}$$

$$X_h = (M_x \cdot cos(\varphi)) - (M_y \cdot sin(\phi) \cdot sin(\varphi)) + ... \quad (M_z \cdot cos(\phi) \cdot cos(\varphi)) \tag{12}$$

$$\psi = atan\frac{Y_h}{X_h} \tag{13}$$

where, M_x, M_y and M_z represent X, Y and Z-axial magnetometer measurements from the sensor, respectively. 9-axis IMU chip (MPU9250, Invensense) is used to estimate the orientation of the sensor. This chip features three 16-bit analog-to-digital (ADC) for gyroscope outputs, three 16-bit ADC for accelerometer outputs and three 16-bit ADC for magnetometer output. For the communication, the I^2C is selected with a sampling rate of 4 kHz.

C. Implementation

Based on the aforementioned configurations and the arrangement of the sensing elements, a 6-axis F/T sensor was designed. The mechanical parts were manufactured through conventional machine works and surface was treated through anodizing to prevent electromagnetic noises. Figure 4. (a) shows the manufactured sensing PCB which embeds IMU sensor in the front and CDC sensors in back. The sensing PCB is installed through a via bolting connection. (Fig. 4 (b)) Figure. 5 illustrates the assembly of the 6-axis F/T sensor. Figure 5. (a) shows the are assembly of deformable plate and bottom plate. In this step, the capacitance is generated between the sensing plate and the sensing PCB. Finally, Fig. 5. (b) shows fully assembled 6-axis F/T sensor. The physical dimensions, sampling rate and force measuring range are listed as in Table I.

III. AUTONOMOUS WEIGHT COMPENSATION (AWC) TECHNIQUE

A. AWC process based on ANN model

To compensate the F/T offsets from the attached tool, 6-axis F/T and estimated roll, pitch, and yaw angle are utilized. The relationship between 6-axis F/T and the F/T offsets from the attached tool can be obtained through use of adjoint transformation as follows [16]:

$$\boldsymbol{FT}_c = \boldsymbol{FT}_r + \boldsymbol{FT}_i \tag{14}$$

Here, $\boldsymbol{FT}_c$ represents the measured F/T which are expressed relative to sensor frame $\{S\}$. $\boldsymbol{FT}_r$ and $\boldsymbol{FT}_i$ represent the calculated reference F/T offsets and pure interacted F/T respectively. $\boldsymbol{FT}_r$ can calculate as follows:

$$\boldsymbol{FT}_r = \begin{bmatrix} \boldsymbol{R}_{BS} & 0 \\ -\boldsymbol{R}_{BS}\hat{\boldsymbol{P}}_T & \boldsymbol{R}_{BS} \end{bmatrix} \boldsymbol{FT}_T \tag{15}$$

$$\boldsymbol{FT}_T = \begin{bmatrix} 0 & 0 & m_t g & 0 & 0 & 0 \end{bmatrix}^T \tag{16}$$

$\boldsymbol{R}_{BS}$ represents the rotation matrix from base frame $\{B\}$ to sensor frame $\{S\}$. $\hat{\boldsymbol{P}}_T$ represents the skew-symmetric matrix of the vector $\boldsymbol{P}_T$ which express the center of mass. $\boldsymbol{FT}_T$ represents the weight force vector.

In the previous researches, the $\boldsymbol{FT}_r$ is calculated according to the above equations [11], [12]. In this letter, the ANN model is applied to estimate the F/T offsets ($\boldsymbol{FT}_g$) as shown in Fig. 6. The 6-axis F/T and estimated roll, pitch, yaw are the inputs of the ANN model and the reference F/T offsets ($\boldsymbol{FT}_r$) is the target of the ANN model. The ANN model consists of two hidden layers and 6 output layers. The weights, bias and non-linear activation functions of each layer are determined based on the calibration process.

$$w_{n,i+1} = w_{n,i} - \gamma \frac{\delta E}{\delta FT_{c,i}} [f'(activeF)]^n z_{1,i} \tag{17}$$

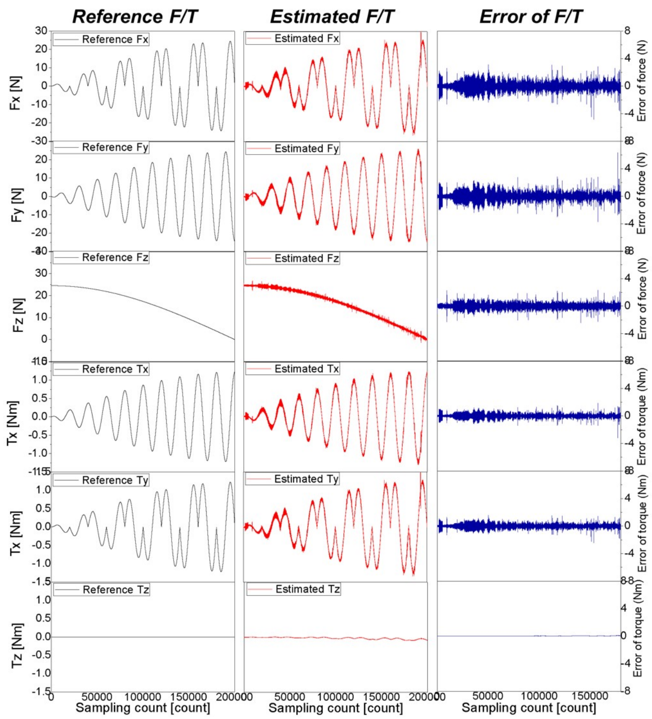

Fig. 9. Calibration result of training data: black line shows the reference F/T, red line shows the estimated F/T, and blue line shows the errors of F/T

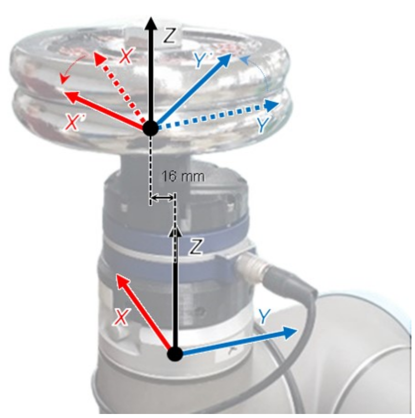

Fig. 10. Evaluation set-up used to obtain Z-axial torque data.

where, w denotes the a weight of ANN model and it subscripts n and i represents states at the i^{th} iteration. $z_{1,i}$ is referred to as the hidden layer. The $i+1^{th}$ weight is updated through the error back propagation using i^{th} parameters. $E = |\boldsymbol{FT}_r - \boldsymbol{FT}_g|$ is expressed as the absolute difference between the reference F/T ($\boldsymbol{FT}_r$) and the estimated F/T ($\boldsymbol{FT}_g$). For the non-linear activation function, the logistic sigmoid function is applied as follow.

$$f_{sigmoid}(x) = \frac{1}{1+e^{-x}} \tag{18}$$

TABLE II
ERROR IN TRAINED DATA SET

	Trained max N, Nm	%(FSO)
F_x	1.840	0.484
F_y	6.356	0.636
F_z	2.427	0.243
T_x	0.318	0.795
T_y	0.242	0.605
T_z	0.009	0.023

B. Data Training

To obtain the training data set, 'UR10' robot manipulator was used to provide orientations and positions to the sensor as shown in Fig. 7. The proposed 6-axis F/T sensor was connected to the end-effector of the manipulator. A dummy tool is attached to the sensor which is consisted of two loads of 1kg, 3D printed parts, bolts, and nuts. Totally, the weight of dummy tool is 2,216 g. In this experiment, the spherical helix path is applied to achieve various orientations of the robot arm. Through this process, various ratios of force vectors are measured from the sensor depending on the gravity applied to the dummy tool.

Fig. 8 presents the result of the estimated Euler angle. The reference Euler angle (black line) is calculated through the rotation matrix from the manipulator and the estimated Euler angle (red line) show the calculated Euler angle based on Eq. (8), (9) and (13).

According to the ANN model conducted to estimate the F/T offsets of the dummy tool, we can calculate the pure interacted F/T by subtracting the estimated F/T from the measured F/T as shown in the equation below:

$$\boldsymbol{FT}_g \simeq \boldsymbol{FT}_r \tag{19}$$

$$\boldsymbol{FT}_i \simeq \boldsymbol{FT}_c - \boldsymbol{FT}_g \tag{20}$$

where $\boldsymbol{FT}_g$ represents the estimated F/T offsets of dummy tool. Consequently, the sensor can export the pure interacted F/T without any manual works and also, additional computing time is not demanded.

Fig. 9 presents the result of the proposed method. The reference F/T ($\boldsymbol{FT}_r$) (black line) represents calculated F/T using rotation matrix from the manipulator and F/T offsets (red line) using equation (14). The known dummy tool's weight, the center of mass and the rotation matrix from UR10 are used to calculate the reference F/T. The estimated F/T ($\boldsymbol{FT}_g$) (red line) shows the results of the proposed ANN model. The blue line presents the differences between reference F/T and estimated F/T. As it shows, the result from proposed ANN model is almost matches with the reference F/T. The maximum F/T offset are summarized as in Table II. It shows, the maximum force error is under 0.7 of %FSO (Full-Scale Output) and the maximum torque error is under 0.8 of %FSO.

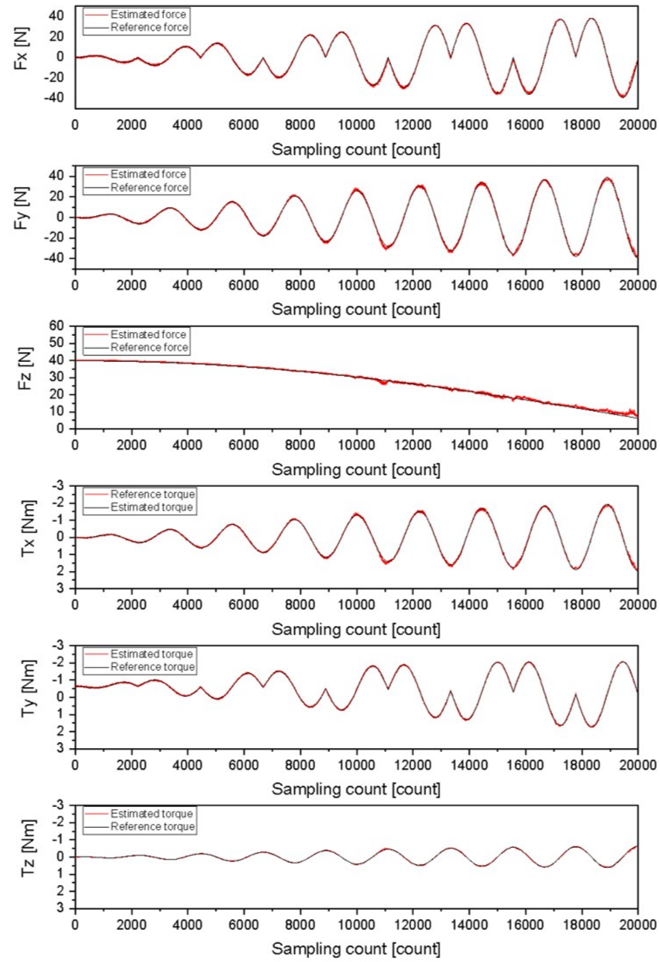

Fig. 11. Calibration result of training data: black line shows the reference F/T, red line shows the estimated F/T.

The Z-axial torque also can be estimated based on the proposed method. To train Z-axial torque, another evaluation set-up was installed to the UR10.(Fig 10) In this set-up, the loads are placed 16 mm apart from the center in X-axis. Also, 4 kg loads are installed to applied Z-axial. Thus, approximately 0.67 Nm can be applied to Z-axial torque.

Fig. 11 presents the result from the second set-up. The reference F/T ($\boldsymbol{FT}_r$) (black line) represents calculated F/T using rotation matrix from the manipulator and F/T offsets(red line) using equation (14). As it shows, the proposed method could estimate the Z-axial torque.

IV. EVALUATION

To verify the reliability of the proposed method, the result should be verified with untrained data. Also, the experiment was conducted through the first evaluation set-up. To obtain the untrained data set, the manipulator is moved in X, Y axis as shown in Fig. 12. The result based on the untrained data is presented in Figs. 13 and

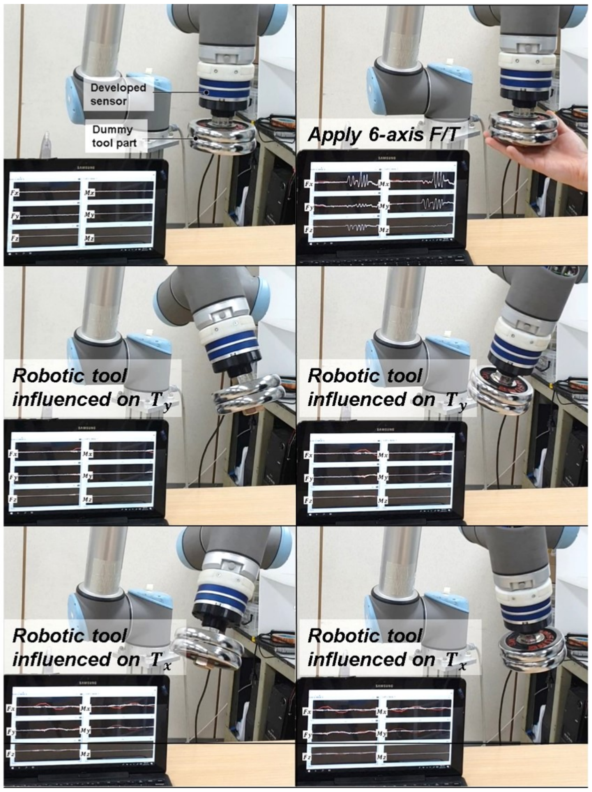

Fig. 12. Experimental images during the evaluation experiment: X, Y axial F/T offsets are occurred due to the attached dummy tool.

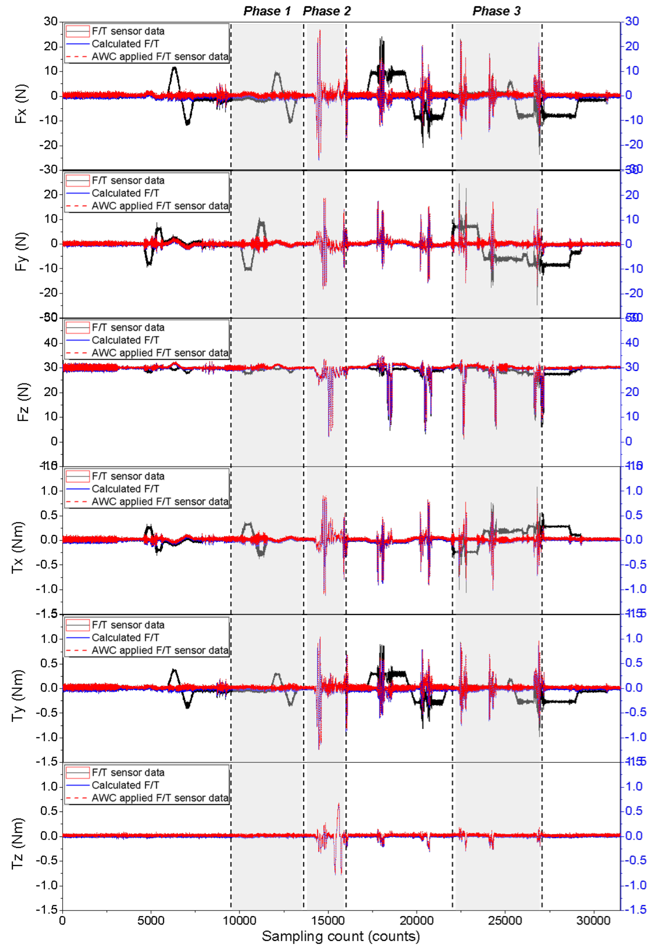

Fig. 13. Experimental results during the evaluation: X, Y axial F/T offsets
are occurred due to the attached dummy tool.

Fig. 14. This result presents three phases to compare the effectiveness of the proposed method.

In Figs. 13 and Fig. 14, the black line represents the measured F/T data including F/T offsets from the attached dummy tool ($\boldsymbol{FT}_c$), the blue line represents the calculated F/T which indicates the reference F/T offset is subtracted from the measured F/T data ($\boldsymbol{FT}_c - \boldsymbol{FT}_r$). The reference F/T offset is obtained by using known weight, center of mass and the rotation matrix. This method is traditional strategy that is introduced in the introduction section. Red-dot-line represents the AWC applied F/T value ($\boldsymbol{FT}_c - \boldsymbol{FT}_g$). In the first phase, the gravity of the dummy tool only affects to the sensor. In other words, any external interaction is not applied to the sensor. As shown in Fig. 14, the black line shows 6-axis F/T offset as a result of the attached dummy tool. The blue line shows that the F/T offset of the attached dummy tool is compensated by subtracting reference F/T offset. Here, the red-dot-line shows that the AWC applied sensor data. As it shows the data is almost fitted with the blue line which indicates it successfully reduces the 6-axis F/T offset from the attached dummy tool. The errors in each phase are listed as in Table III. In the first phase the maximum force error between ($\boldsymbol{FT}_c - \boldsymbol{FT}_r$) and ($\boldsymbol{FT}_c - \boldsymbol{FT}_g$) is under 0.9 of $\%FSO$ and the maximum torque error is under 0.15 of $\%FSO$.

In the second phase, the dummy tool is headed to Z-axis. Hence, only the Z-axial gravity force is applied to the sensor while the external 6-axis F/T is indiscriminately acted to the sensor. In this phase, it shows that the AWC applied sensor data and the original sensor data measure the same 6-axis F/T values. In the second phase the maximum force error is under 1.1 $\%FSO$ and the maximum torque error is under 1 $\%FSO$.

Finally, In the third phase, the axial F/T offsets and the interaction 6-axis F/T are applied simultaneously. The black line shows the measured F/T are also influenced by the F/T offsets. Conversely, the red-dot-line shows that the sensor can measure the pure interaction F/T regardless of the gravity effected on the dummy tool. In the third phase, the maximum force error is under 0.7 of $\%FSO$ and the maximum torque error is under 0.8 of $\%FSO$.

V. CONCLUSIONS

This letter proposes a 6-axis F/T sensor that is capable of novel Autonomous Weight Compensation (AWC)technique. For the 6-axis F/T sensing, eight capacitance values are used and for the orientation estimation, the Euler angles are used which can be calculated by

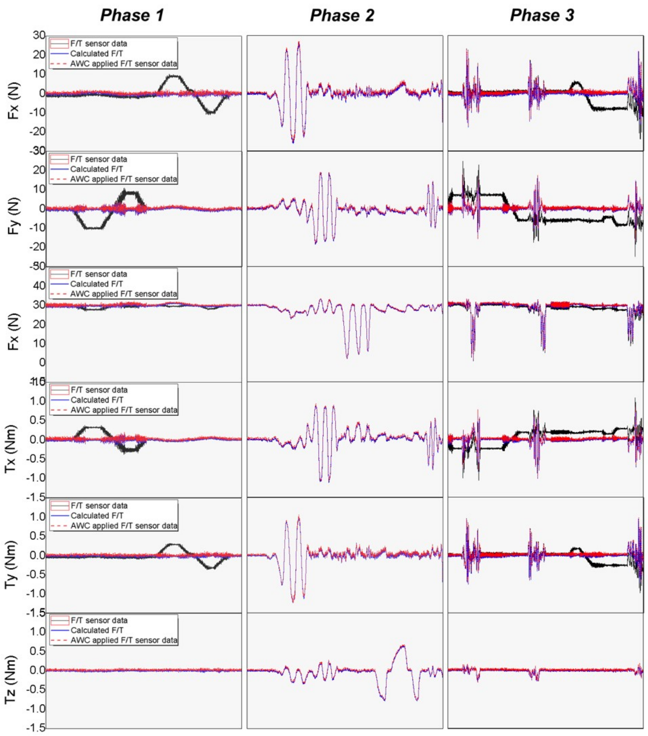

Fig. 14. Expanded results in three phases.

TABLE III
ERROR IN UNTRAINED DATA SET

	Untrained max					
	Phase 1		Phase 2		Phase 3	
	N, Nm	$\%(FSO)$	N, Nm	$\%(FSO)$	N, Nm	$\%(FSO)$
F_x	4.323	0.859	4.431	1.049	3.554	0.638
F_y	3.592	0.718	3.303	0.661	3.323	0.665
F_z	0.564	0.113	1.060	0.212	0.947	0.189
T_x	0.028	0.140	0.172	0.858	0.135	0.673
T_y	0.013	0.063	0.190	0.949	0.152	0.760
T_z	0.007	0.035	0.126	0.630	0.026	0.129

using installed 9-axis IMU sensor. To achieve the simple manufacturing work and easy assembly process, the developed sensor consists of four mechanical parts and one signal processing board. ANN model is implemented to overcome the F/T offsets resulting from the attached tool. Finally, the performance of the proposed sensor is verified through experiments using training data and untrained test data sets. The experiments involve using 'UR10' manipulator and a dummy tool. The result shows that a maximum of 0.8 of $\%FSO$ of F/T offsets is occurred in estimating the F/T offsets resulting from the attached dummy tool. In the untrained test data, it shows the F/T offsets resulting from the dummy tool is maximally 1.1 of $\%FSO$ which indicates the sensor can autonomously compensate the F/T offsets itself. In this research, we focused to compensate F/T offsets based on static analysis. Thus, quasi-static motion is not considered in this letter, the reason is that the work using 6-axis F/T sensors is mostly purposed for high accuracy of human-robot collaboration rather than fast speed. Also, in this study, we focused to embed the AWC method inside of the sensor to resolve the F/T offsets from the attached tools. For the future work, quasi-static relation will be considered to update in AWC method to compensate the F/T offset completely.

References

[1] F.Dimeas, V. C. Moulianitis, C. Papakonstantinou and N. Aspragathos, "Manipulator Performance Constraints in Cartesian Admittance Control for Human-Robot Cooperation", IEEE Int. Conf. on Robot. Autom. (ICRA), pp. 222 - 233, 2018.

[2] K. Watanabe, T. Kanno, K. ito, and K. Kawashima, "Single-Master Dual-Slave Surgical Robot With Automated Relay of Suture Needle", IEEE Trans. Ind. Electron., vol. 65, no. 8, pp. 6343 - 6351, 2018.

[3] A. D. Luca, A. Albu-Schaffer, S. Haddadin, D. Hirzinger, "Collision Detection and Safe Reaction with the DLR-III Lightweight Manipulator Arm", IEEE/RSJ Int. Conf. Robot. Syst (IROS), pp. 1623 - 1630, 2006.

[4] S. Haddadin, A. D. Luca, A. Albu-Schaffer, "Robot Collisions: A Survey on Detection, Isolation, and Identification", IEEE Trans. Robot., vol. 33, no. 6, pp. 1292 - 1312, 2017.

[5] Y. -L. Park, S. C. Ryu, R. J. Black, K. K. Chau, B. Moslehi, and M. R. Cutkosky, "Exoskeletal Force-Sensing End-Effectors With Embedded Optical Fiber-Bragg-Grating Sensors," IEEE Trans. Robot., vol. 25, no. 6, pp. 1319 - 1331, 2009.

[6] Y. B. Kim, U. Kim, D. -Y. Seok, J. So, Y. H. Lee and H. R. Choi, "Torque Sensor Embedded Actuator Module for Robotic Applications", IEEE/ASME Trans. Mech., vol. 2, no. 4, pp. 1662 - 1672, 2018.

[7] Y. H. Lee, Y. H. Lee, H. Y. Lee, H. Kang, L. T. Phan, S. Jin, Y. B. Kim, D. -Y. Seok, S. Y. Lee, "Force-controllable Quadruped Robot System with Capacitive-type Joint Torque Sensor", IEEE Int. Conf. on Robot. Autom. (ICRA), pp. 6777 - 6782, 2019.

[8] U. Kim, Y. B. Kim, D. -Y. Seok, J. So and H. R. Choi, "A Surgical Palpation Probe With 6-Axis Force/Torque Sensing Capability for Minimally Invasive Surgery", IEEE Trans. Ind. Electron., vol. 65, no. 3, pp. 459 - 460, 2018.

[9] R. Hazelden, "Optical torque sensor for automotive steering systems," Sensors and Actuators A: Physical, vol. 37, pp. 193 - 197, 1993.

[10] D.-Y. Seok, Y. B. Kim, U. Kim, S. Y. Lee and H. R. Choi, "Compensation of Environmental Influences on Sensorized-Forceps for Practical Surgical Tasks," in IEEE Robot. Autom. Letter(RA-L), pp. 2031 - 2037, 2019.

[11] "Start Production Faster," Robotiq. [Online]. Available: https://robotiq.com/. [Accessed: 12-Oct-2019].

[12] F. Dimeas, N. Asparagathos, "Learning optimal variable admittance control for rotational motion in human-robot co-manipulation," IFAC-PapersOnLine, vol. 48, no. 19, pp. 124 - 129, 2015.

[13] W. Y. Kim, S. Y. Ko, J, -O. Park, and S. Park, "6-DOF force feedback control of robot-assisted bone fracture reduction system using double F/T sensors and adjustable admittances to protect bones against damage,"Mechatronics, vol. 35, pp. 136-147, 2016.

[14] L. Richter, R. Bruder, A. Schweikard, " Calibration of Force/Torque and Acceleration for an Independent Safety Layer in Medical Robotic Systems,"Cureus, vol. 4 no. 9, 2012.

[15] U. Kim, D.-H. Lee, Y. B. Kim, D.-Y. Seok, and H. R. Choi, " A novel six-axis force/torque sensor for robotic applications," IEEE/ASME Trans. Mech., vol. 22, no. 3, pp. 1381 - 1390, 2017.

[16] R. M. Murray, Z. Li, and S. S. Sastry, "A Mathematical Introduction to Robotic Manipulation," CRC Press., 1994.

[17] H. S. Oh, U. Kim, G. Kang, J. K. Seo and H. R. Choi, "Multi-Axial Force/Torque Sensor Calibration Method Based on Deep-Learning," IEEE Sensors, vol. 18, no. 13, pp. 5485 - 5496, 2018.